PHY-3610-1, Statistical Mechanics
Ashoka University, Monsoon 2020

Comparative analysis of Monte Carlo path integrals and perturbation theory for the quantum quartic-anharmonic oscillator

Tatsam Garg
Ashoka University

Instructors
Prof. Vikram Vyas
Ms. Manmeet Kaur

December 11th, 2020

Acknowledgements

I'd like to thank my instructor Prof. Vikram Vyas for his patient guidance. He has continued to motivate me to approach physics with curiosity and rigor. I express my gratitude to Ms. Manmeet who helped me troubleshoot my code and guided me through doubts, and Prof. Amin A. Nizami for special assistance on asymptotic perturbative expansions and correlation functions.

Contents

1. Introduction

Schrödinger's wave mechanics formulation of quantum mechanics is a mainstay of the physics undergraduate curriculum. However, at times, analytical solutions to Schrödinger's equations may not be possible. Perturbation theory allows for approximate solutions, but the framework breaks down for large perturbations. For certain cases, particularly the ones with manifest Lorenz covariance, path integrals are a useful approach to quantum mechanics. Unfortunately, analytical solutions to this framework are significantly challenging. Thus, we turn to numerical solutions. A special motivation for this is that the Monte Carlo method has a direct correspondence to the canonical ensemble of statistical mechanics. Thus, we're able to draw a connection between the physical properties of the quantum theory and statistical physics.

In this study, we want to explore how quantum mechanical problems that are typically difficult to solve analytically in the Schrödinger framework, and not always have reliable perturbative solutions, can be formulated into the path integral framework. We will solve them using the Markov Chain Monte Carlo

(MCMC) method, drawing an analogy between the path integral and the canonical partition function. We will explore how the Monte Carlo method uses this correspondence to find various correlation functions from the statistical theory that can yield physical observables. To make this analysis, we use the familiar one-dimensional quantum harmonic oscillator. It is physically relevant because any system near a local stable equilibrium can be approximated as such. To make the approximation more realistic, higher order corrections can be added to the potential. We consider the quartic correction to the harmonic potential. We compare the perturbative solutions for the ground and first excited state energies with MCMC solutions and illustrate the instability of the perturbative solutions versus the stability of numerical solutions, thus, exploring a powerful numerical alternative to analytically difficult problems.

2. Quantum oscillators

2.1. Harmonic potential

The one-dimensional quantum harmonic oscillator is subject to a harmonic potential of the form:

$$V(x) = ax^2 \qquad \ldots(1)$$

The Hamiltonian of this system in the position basis is given by:

$$\widehat{H} = -\frac{\hbar^2}{2m}\frac{d^2}{dx^2} + \frac{m\omega^2 x^2}{2} \qquad \ldots(2)$$

Where m is the mass, ω is the natural frequency and x is the position of the oscillator. The action of the Hamiltonian on an energy eigenfunction, ψ, for energy E gives the Schrödinger time-independent equation.

$$\widehat{H}\psi = \left(-\frac{\hbar^2}{2m}\frac{d^2}{dx^2} + \frac{m\omega^2 x^2}{2}\right)\psi = E\psi \qquad \ldots(3)$$

The solution of this second order ordinary differential equation requires us to find the energy eigenvalues and the normalizable energy eigenfunctions of the system. This can either be done using the power series method to find a wavefunction in terms of Hermite Polynomials or using a rather non-intuitive algebraic method by constructing special lowering and raising operators which generate the entire spectrum of the quantum harmonic oscillator.

The energy eigenvalues for the n^{th} excited state of this system are given by:

$$E_n = \hbar\omega\left(n + \frac{1}{2}\right)$$

…(4)

For $n \in \{0, 1, 2, 3 \ldots\}$. The energy eigen-function in the n^{th} excited state is

$$\psi_n(x) = \left(\frac{m\omega}{\pi\hbar}\right)^{\frac{1}{4}} \frac{1}{\sqrt{2^n n!}} H_n(\xi) e^{-\xi^2/2}$$

…(5)

Where $\xi \equiv \sqrt{\frac{m\omega}{\hbar}}x$, $H_n(\xi)$ are Hermite polynomials. Therefore, for the ground and the first excited states, the energy eigen-functions take the following form:

$$\psi_0(x) = \left(\frac{m\omega}{\pi\hbar}\right)^{\frac{1}{4}} e^{-\frac{m\omega}{2\hbar}x^2}$$

…(6)

$$\psi_1(x) = \left(\frac{m\omega}{\pi\hbar}\right)^{\frac{1}{4}} \sqrt{\frac{2m\omega}{\hbar}}\, x\, e^{-\frac{m\omega}{2\hbar}x^2}$$

…(7)

Thus, in the ground state, we expect a gaussian wavefunction.

2.2. Non-degenerate Perturbation Theory

Perturbation theory develops a framework for approximating solutions to analytical problems when a small perturbation is introduced into the original problem, rendering it difficult or even impossible to be solved using analytical methods. In the context of quantum mechanics, consider a usual unperturbed Hamiltonian, H^0, perturbed by an arbitrary operator, H'. Note the emphasis on the fact that H' is a mere perturbation, therefore, it is coupled weakly to H^0. The net perturbed Hamiltonian becomes:

$$H = H^0 + \lambda H'$$

…(8)

where λ is a small coupling parameter. H has leading contributions from H^0. Perturbation theory allows us to write the energy eigenvalues and energy eigen-functions of this new perturbed Hamiltonian as a power series of the coupling constant.

$$E_n = E_n^0 + E_n^1\lambda + E_n^2\lambda^2 + E_n^3\lambda^3 + \cdots$$

…(9)

$$\psi_n = \psi_n^0 + \psi_n^1\lambda + \psi_n^2\lambda^2 + \psi_n^3\lambda^3 + \cdots$$

…(10)

Here, E_n^0 and ψ_n^0 are the energy eigenvalues and energy eigen-functions respectively of the unperturbed Hamiltonian H^0. E_n^1 and ψ_n^1 are the first order corrections to the n^{th} eigenvalue and eigen-function respectively. Likewise, E_n^2 and ψ_n^2 are the second order corrections. In principle, we desire to calculate E_n and ψ_n up to the highest order correction possible. This may at times be not true, particularly in the case of asymptotic series. We will discuss this further with an example in the next section.

Using expressions (8), (9) and (10), some amount of algebra allows us to derive expressions for E_n^1, ψ_n^1 and E_n^2.

$$E_n^1 = \langle\psi_n^0|H'|\psi_n^0\rangle$$

…(11)

$$\psi_n^1 = \sum_{m\neq n} \frac{\langle\psi_m^0|H'|\psi_n^0\rangle}{E_n^0 - E_m^0}\,\psi_m^0$$

…(12)

$$E_n^2 = \sum_{m\neq n} \frac{|\langle\psi_m^0|H'|\psi_n^0\rangle|^2}{E_n^0 - E_m^0}$$

…(13)

Expression (11) is often regarded as the fundamental result of first-order perturbation theory. It says that the first order correction to the eigenvalues of the perturbed Hamiltonian is given by the expectation value of the perturbation in the unperturbed eigenstate corresponding to the eigenvalue. We use expressions (11) and (13) to calculate the ground state and first excited state energies up to the second-order perturbative expansion for the quartic anharmonic oscillator in the next section.

2.3. Quartic anharmonic potential

We consider a quantum harmonic oscillator perturbed by a quartic anharmonic potential. The Hamiltonian takes the following form:

$$\widehat{H} = -\frac{\hbar^2}{2m}\frac{d^2}{dx^2} + \frac{m\omega^2x^2}{2} + \lambda x^4$$

…(14)

Comparing with (8),

$$\widehat{H}^0 = -\frac{\hbar^2}{2m}\frac{d^2}{dx^2} + \frac{m\omega^2x^2}{2}$$

…(15)

$$\widehat{H}' = x^4$$

…(16)

Substituting (16) in (11),

$$E_n^1 = \langle \psi_n^0 | x^4 | \psi_n^0 \rangle$$

Note that $\widehat{H}'$ and x^4 are not in the same units. Therefore, we transform x^4 into units of energy using a characteristic length scale $d = \hbar/m\omega$. Using the raising and lowering operator notation to replace the position operator,

$$\Rightarrow E_n^1 = \frac{\hbar\omega}{4}\left\langle \psi_n^0 \middle| \left(\hat{a}^\dagger + \hat{a}\right)^4 \middle| \psi_n^0 \right\rangle$$

We expand the bracketed term and compute the effects of the operators on $|\psi_n^0\rangle$. 16 terms are obtained. Upon computing the inner product with $\langle \psi_n^0 |$, only those terms survive which contain $|\psi_n^0\rangle$. We get

$$\frac{\hbar\omega}{4}\left\langle \psi_n^0 \middle| \left(\hat{a}^\dagger + \hat{a}\right)^4 \middle| \psi_n^0 \right\rangle = \frac{\hbar\omega}{4}\begin{bmatrix} n(n-1) + n^2 + n(n+1) + n(n+1) \\ + \\ (n+1)^2 + (n+1)(n+2) \end{bmatrix}$$

$$\Rightarrow E_n^1 = \frac{3}{4}\hbar\omega(2n^2 + 2n + 1)$$

…(17)

Expression (17) gives the first order perturbative correction to the energy of the n^{th} excited state. Next, we compute the second order perturbative correction to the ground state energy.

$$E_0^2 = \left(\frac{\hbar\omega}{d^4}\right)^2 \sum_{m\neq 0} \frac{|\langle \psi_m^0 | x^4 | \psi_0^0 \rangle|^2}{E_0^0 - E_m^0}$$

$$\Rightarrow E_0^2 = \left(\frac{\hbar\omega}{4}\right)^2 \sum_{m\neq 0} \frac{\left|\left\langle \psi_m^0 \middle| \left(\hat{a}^\dagger + \hat{a}\right)^4 \middle| \psi_0^0 \right\rangle\right|^2}{E_0^0 - E_m^0}$$

As we did for E_n^1, the expansion of the operator yields

$$\left(\hat{a}^\dagger + \hat{a}\right)^4 |\psi_0^0\rangle = 3|\psi_0^0\rangle + 6\sqrt{2}|\psi_2^0\rangle + \sqrt{4!}\,|\psi_4^0\rangle$$

$$\Rightarrow \left(\frac{\hbar\omega}{4}\right)^2 \sum_{m\neq 0} \frac{\left|\left\langle \psi_m^0 \middle| \left(\hat{a}^\dagger + \hat{a}\right)^4 \middle| \psi_0^0 \right\rangle\right|^2}{E_0^0 - E_m^0} = -\frac{(\hbar\omega)^2}{2\hbar\omega}\frac{9}{2} - \frac{(\hbar\omega)^2}{4\hbar\omega}\frac{3}{2}$$

$$\Rightarrow E_0^2 = -\frac{21}{8}\hbar\omega$$

…(18)

Similarly, we compute the second order perturbative correction to the first excited state energy.

$$E_1^2 = \left(\frac{\hbar\omega}{d^4}\right)^2 \sum_{m\neq 1} \frac{|\langle \psi_m^0 | x^4 | \psi_1^0 \rangle|^2}{E_1^0 - E_m^0}$$

$$\Rightarrow \left(\frac{\hbar\omega}{4}\right)^2 \sum_{m\neq 1} \frac{\left|\left\langle \psi_m^0 \middle| \left(\hat{a}^\dagger + \hat{a}\right)^4 \middle| \psi_1^0 \right\rangle\right|^2}{E_1^0 - E_m^0} = \frac{\hbar\omega}{16}\left[\frac{5!}{4} + 3 + 12 + 27 + 48\right]$$

$$\Rightarrow E_1^2 = -\hbar\omega\frac{15}{2}$$

…(19)

Finally, putting (4), (17), (18) and (19) together, the full ground and first excited state energies for the quartic-perturbed Hamiltonian up to second order perturbative corrections are given by:

$$E_0 = \frac{\hbar\omega}{2}\left(1 + \frac{3}{2}\lambda - \frac{21}{4}\lambda^2\right)$$

…(20)

$$E_1 = \frac{\hbar\omega}{2}\left(3 + \frac{15}{2}\lambda - 15\,\lambda^2\right)$$

…(21)

In general, these expansions can be determined up to higher order corrections, albeit with great difficulty, and not always leading to appreciable applicability. Bender and Wu (Phys. Rev.184 (1969)1231) [8] computed the expansion for the ground state energy E_0 of the Hamiltonian under study up to several higher order corrections. The expansion up to the sixth order is as follows:

$$E_0(\lambda) = \frac{\hbar\omega}{2}\left(1 + \frac{3}{2}\lambda - \frac{21}{4}\lambda^2 + \frac{333}{8}\lambda^3 - \frac{30885}{64}\lambda^4 + \frac{916731}{128}\lambda^5 - \frac{65518401}{512}\lambda^6 + \mathcal{O}(\lambda^7)\right)$$

…(22)

The radius of convergence of this series is zero. The coefficients keep growing and the series does not converge for any non-zero value of λ. This is an asymptotic expansion. Of course, such expansions are

not useless. Specific methods allow isolation of sections which have more significant and convergent contribution to the series. Typically, one may calculate the successive terms as long as they keep decreasing. If successive terms start to increase, we may truncate the expansion. In our study, even though the expansion was used only up to the second order correction, we were restricted to values of $\lambda < 0.2$ to obtain meaningful perturbed-energy values. For larger coupling parameters, the perturbative solutions became unstable. Our analysis of the asymptotic series is briefly illustrated in the results. The numerical approach that we shall discuss next rectifies this limitation of perturbation theory. Since the foundation of perturbation theory is within expression (9) and (10), it is strictly restricted to regimes of λ within which such expansions can be defined. For larger λ, the framework breaks down even for higher order corrections as we can't assume the expansions (9) and (10). This, of course, is not a limitation for numerical methods as we will see in the subsequent sections.

3. Path integrals and partition functions

3.1. The Feynman path integral

We're familiar with the popular Hamiltonian and Lagrangian formulations of classical mechanics. The Schrödinger formulation that we have discussed for quantum mechanics is analogous to the Hamiltonian approach since, in this framework, the Hamiltonian generates time evolution in the system via the Schrödinger time-dependent equation

$$i\hbar \frac{\partial \psi}{\partial t} = \hat{H}\,\psi \qquad \ldots(23)$$

Suppose we start from an initial state $\psi(x, 0)$. Solving (23) gives the state at a later time *t* as the action of a unitary time evolution operator on the initial state.

$$\psi(x, t) = e^{-i\hat{H}\frac{t}{\hbar}}\,\psi(x, 0) \qquad \ldots(24)$$

Therefore, the probability amplitude of a particle starting at x_i, t_i and evolving to x_f, t_f can be expressed as the following inner product yielding a matrix element of the time evolution operator:

$$\langle x_f, t_f | x_i, t_i \rangle = \left\langle x_f \middle| e^{-i\hat{H}(t_f - t_i)/\hbar} \middle| x_i \right\rangle \qquad \ldots(25)$$

This quantity is defined as the propagator. It is an essential quantity to describe time evolution. While we motivated it from the Hamiltonian formulation, Feynman's path integral approach allows us to define the propagator in terms of the Lagrangian. As opposed to the classical case, where we can deterministically infer that the particle must take the path which extremizes the action (principle of least action), for obvious reasons, this can not be inferred for quantum mechanical particles. Thus, we

consider the contribution from all possible paths, each weighted by a phase factor determined by the classical action for that path. The Feynman path integral is, therefore, defined as:

$$\left\langle x_f \middle| e^{-i\hat{H}(t_f - t_i)/\hbar} \middle| x_i \right\rangle = \int \left(Dx(t) \exp\left[-\frac{i}{\hbar} \int_{t_i}^{t_f} L\big(x(t)\big) dt \right] \right) \quad \ldots(26)$$

Where $Dx(t)$ denotes an integral over all space-time paths (x, t) between (x_i, t_i) and $\left(x_f, t_f\right)$. L is the classical Lagrangian while $S = \int_{t_i}^{t_f} L\big(x(t)\big) dt$ is the classical action.

$$L\big(x(t)\big) = \frac{m}{2}\left(\frac{dx}{dt}\right)^2 - V\big(x(t)\big) \quad \ldots(27)$$

3.2. Imaginary time

Recall that our considerations for paths have been in space-time dimensions. Therefore, we've been following the Minkowski metric. It becomes equivalent to the Euclidean metric if time is allowed to take only imaginary values. Since Euclidean space offers easier computations and geometry, we make the following transformation in (26), also known as the Wick rotation:

$$t \to -i\tau$$

To yield

$$\left\langle x_f \middle| e^{-\hat{H}(\tau_f - \tau_i)/\hbar} \middle| x_i \right\rangle = \int \left(Dx(\tau) \exp\left[-\frac{1}{\hbar} \int_{\tau_i}^{\tau_f} L_E\big(x(\tau)\big) d\tau \right] \right) \quad \ldots(28)$$

Where

$$L_E\big(x(\tau)\big) = \frac{m}{2}\left(\frac{dx}{d\tau}\right)^2 + V\big(x(\tau)\big) \quad \ldots(29)$$

We will discretize (28) and (29) for numerical calculations in the subsequent sections. A curious motivation to make the imaginary-time transformation is that it draws a one-to-one mathematical analogy between the path integral and the partition function of quantum statistical mechanics. To see this, we set $x_i = x_f$, $\tau_i = 0$ and $\tau_f = \hbar\beta$ where $\beta = 1/(k_B T)$. Here, k_B is the Boltzmann's constant and T is the absolute temperature.

$$\left\langle x \middle| e^{-\beta\hat{H}} \middle| x \right\rangle = \mathrm{Tr}\left(e^{-\beta\hat{H}}\right)$$

$$\Rightarrow Z = \int \left(Dx(\tau) \exp\left[-\frac{1}{\hbar} \int_0^{\hbar\beta} L_E\big(x(\tau)\big) d\tau \right] \right)$$

…(30)

The trace of $e^{-\beta \hat{H}}$ is the canonical partition function Z. For our simulations of the harmonic oscillator, indeed, we set $x_i = x_f$ and $\tau_i = 0$. Therefore, it's interesting to see that a Monte Carlo program used to calculate the path integral can also double as a program to compute the partition function. We will now use Z to construct correlation functions that will yield physical observables, particularly the ones we are interested in— the ground and first excited state energies.

3.3. Correlation functions

Physical observables are encoded in correlation functions which are the expectation values of products of the position operator. The correlation functions are of the form:

$$\langle \hat{x}(\tau_1)\hat{x}(\tau_2)\hat{x}(\tau_3) \dots \hat{x}(\tau_n) \rangle = \frac{1}{Z} \operatorname{Tr}[\mathrm{e}^{-\beta \hat{H}} \hat{x}(\tau_1)\hat{x}(\tau_2)\hat{x}(\tau_3) \dots \hat{x}(\tau_n)]$$

…(31)

Now, compare the form of (31) with that of the Boltzmann probability distribution of paths created in our Monte Carlo simulation using the metropolis algorithm.

$$P[x(\tau)]Dx(\tau) = \frac{1}{\int \mathrm{e}^{-\frac{S}{\hbar}} Dx(\tau)} \mathrm{e}^{-\frac{S}{\hbar}} Dx(\tau)$$

…(32)

The denominator on the RHS is like a path integral, which we have shown to be equal to Z in (30). Using this probability distribution, if we find the average of any quantity of the form $\hat{x}(\tau_1) \dots \hat{x}(\tau_n)$, we get the expression (31). Therefore, an average of $\hat{x}(\tau_1) \dots \hat{x}(\tau_n)$ over all the paths in the probability distribution (32) will allow us to calculate a statistical correlation function, and thus, physical observables! This is the deep connection between path integrals and statistical mechanics that warrants our interest in this study. To sum up our approach for the rest of the analysis, we use the path integral to motivate a probability distribution of a large number of paths. Next, motivated by the analysis of statistical physics, we compute the average of certain quantities like $\hat{x}(\tau_1) \dots \hat{x}(\tau_n)$ over all these paths. These averages are equivalent to the correlation functions, and thus, will let us calculate physical observables and other properties.

In our study, we're interested in the ground state and the first excited state energy of the quantum harmonic and anharmonic oscillator. Using the virial theorem of quantum mechanics, the Hamiltonian (14) for a quartic-anharmonic oscillator in the large time, or equivalently, $\beta \to \infty$ limit gives

$$E_0 = m\omega \langle \hat{x}^2 \rangle + 3\lambda \langle \hat{x}^4 \rangle$$

…(33)

Thus, this correlation function for our path ensemble following the Boltzmann probability distribution will allow us to calculate the ground state energies for various values of the perturbative coupling λ. Next, we construct the following correlation function:

$$G(\tau) \equiv \langle\langle \hat{x}(\tau_1)\hat{x}(\tau_2)\rangle\rangle \quad \ldots(34)$$

Where $\tau = \tau_2 - \tau_1$. The double brackets denote double averaging— once over a single path for all $x_i = x_f$, and then over the entire ensemble of paths. In the large total time, or equivalently, $\beta \to \infty$ limit, the ground state dominates:

$$\lim_{\beta\to\infty} G(\tau) = \sum_{n=1}^{\infty} e^{-(E_n - E_0)\tau/\hbar}\, |\langle 0|\hat{x}|n\rangle|^2$$

And in the large τ limit,

$$\lim_{(\tau_2-\tau_1)\to\infty} \left[\frac{\mathrm{d}\log\big(G(\tau)\big)}{d\tau}\right] = E_1 - E_0$$

Therefore, after taking the above limits and integrating, for a time step *a*:

$$\log\left(\frac{G(\tau)}{G(\tau + a)}\right) = (E_1 - E_0)a \quad \ldots(35)$$

Thus, $G(\tau)$ for our path ensemble following the Boltzmann probability distribution will allow us to calculate the difference between the first excited state energy and the ground state using (35).

4. Markov Chain Monte Carlo (MCMC)

Monte Carlo integration allows for estimation of multidimensional integrals by drawing samples from a probability distribution and averaging over a large number of samples. While one may simulate the exact probability distribution, a prominent method to do so is using Markov chains. By definition, a Markov chain is a stochastic model describing a sequence of possible events in which the probability of each event depends only on the state attained in the previous event. After a sufficient number of successive iterations, the Markov chain reaches an equilibrium distribution. This is called thermalization. This equilibrium distribution can be made to replicate the original required probability distribution, and thus, be used for drawing samples. Several algorithms may be used to update the events. In this study, we use the Metropolis algorithm.

We've seen that path integrals are multidimensional integrals over all the possible paths. If we discretize the integral, it's simple to interpret it as a summation over all possible paths, with each path having a weight factor given by the action, *S*, for that path as $\mathrm{e}^{-S/\hbar}$ in the imaginary-time formulation.

Alternatively, the MCMC method seeks to create a set of paths which follow the probability distribution (32) motivated by this weight factor. Therefore, when large number of samples are drawn from this distribution, any individual path will inherently carry the weight factor by the virtue of the probability distribution. Thus, the weighted summation of path integrals is replaced by a simple unweighted summation of paths drawn from the equilibrium probability distribution.

4.1. Metropolis algorithm

We will now review the Metropolis algorithm used for generating the Markov chain of paths in accordance with the probability distribution (32).

- Start with an arbitrary discrete path of *N* lattice points (Initialization).
- Visit each lattice point and randomly update (add) it with some small value δ, which has a uniform probability distribution $-\epsilon < \delta < \epsilon$.
- Upon the update of each lattice point, calculate the new action ΔS. (This will typically be local since Lagrangians are local. Only a few terms in lattice action involve any given lattice point; only these need to be calculated.)
- If $\Delta S < 0$, retain the update and move to the next lattice point.
- If $\Delta S > 0$, retain the update only with probability $\propto \mathrm{e}^{-\Delta S/\hbar}$. That is, if a random number between 0 and 1 is less than $\mathrm{e}^{-\Delta S/\hbar}$, retain the update and proceed. Else restore the previous value and proceed.
- Visiting all lattice points and conducting the above procedure constitutes one Metropolis sweep. After initialization, several Metropolis sweeps are required to attain thermalization— the equilibrium probability distribution.

4.2. Simulation algorithm

Since we update lattice points with a small number $-\epsilon < \delta < \epsilon$ of the order of quantum fluctuations, any two successively generated paths would be highly correlated. This is not ideal for our simulation. Thus, we define a correlation parameter, N_{cor}, which is roughly the number of Metropolis sweeps required to remove the correlation between any two successive paths chosen for analysis.

The algorithm for computing any correlation function $\langle\langle \Gamma[x(\tau)] \rangle\rangle$ is as follows:

- Initialize path. Update path for 5 N_{cor} to 10 N_{cor} Metropolis sweeps to thermalize the lattice.
- Compute $\Gamma[x(\tau)]$ for path, save it, and update the path N_{cor} times. Repeat a large number of times.
- Average over all the saved values of $\Gamma[x(\tau)]$ to obtain the Monte Carlo estimate $\bar{\Gamma}$.

The parameters N, ϵ, N_{cor} and the number of total paths analyzed, N_{cf} , were set as the following using the analysis by Peter G. Lepage in reference [1]:

$$N = 20 \; ; \epsilon = 1.4 \; ; N_{\text{cor}} = 20 \text{ and } 5000 < N_{\text{cf}} < 10^4$$

4.3. Discretization

Numerical calculations required the following discretized quantities:

The total lattice action:

$$S_{\text{lat}}[x] = \sum_{j=0}^{N-1} \left[\frac{m}{2a}\left(x_{j+1} - x_j\right)^2 + aV\left(x_j\right)\right] \quad \ldots(36)$$

Where $a \equiv T/N$, T being the total time; and $V\left(x_j\right) = \frac{m\omega^2 x_j^2}{2} + \lambda x_j^4$ is the full potential including the quartic perturbation.

The local lattice action:

$$S_{\text{loc}}[x] = \frac{m}{2a} x_j\left(x_j - x_{j+1} - x_{j-1}\right) + aV\left(x_j\right) \quad \ldots(37)$$

For ground state energy:

$$\Gamma[x] = \frac{1}{N}\sum_{j=1}^{N}\left(m\omega \, {x_j}^2 + 3\lambda \, x_j^4\right) \quad \ldots(38)$$

For the correlation function in (34):

$$G_n = \frac{1}{N}\sum_{j=1}^{N} \langle\langle x_{(j+n)\%N} \, x_j \rangle\rangle \quad \ldots(39)$$

Where the $\%N$ sign denotes periodic boundary conditions. G_n is a Monte Carlo estimate as indicated by the expectation value on the RHS.

For the first excited state energy:

$$\Delta E_1 = E_1 - E_0 = \frac{1}{a} \log\left(\frac{G_n}{G_{n+1}}\right) \quad \ldots(40)$$

4.4. Statistical errors

The relative standard deviation for the expectation value of a random variable in statistics is widely known to go as:

$$\frac{\sigma_\Gamma}{\langle\Gamma\rangle} \propto \frac{1}{\sqrt{N_{\text{cf}}}} \qquad \ldots(41)$$

We use this relation to plot the error bars in our graphs.

5. Results

For all simulations and results, we set the system parameters as:

$$m = \omega = \hbar = 1$$

Therefore, we obtain the energies in the units of $\hbar$. Before illustrating the results for the MCMC computations, we briefly show the results obtained by directly solving the multidimensional path integral using a standard python package *vegas* to appreciate how the MCMC approach and the path integral approach is indeed equivalent in the statistical limit.

5.1. Direct integration

We solve for the propagator in (28) with the discrete lattice action (36) using the *vegas* package for the ground state of the quantum harmonic oscillator. Note that we set $x_i = x_f$, thus effectively finding the canonical partition function (30). The propagator in the large time limit yields the non-normalized probability density as:

$$\lim_{\beta\to\infty} \langle x|e^{-T\hat{H}}|x\rangle = \mathrm{e}^{-E_0 T}\ |\langle x|0\rangle|^2$$

Therefore, integrating over space isolates the exponential constant. Thus the wavefunction is given by taking the square root:

$$\psi_0 = \langle x|0\rangle = \left(\frac{\lim_{\beta\to\infty} \langle x|e^{-T\hat{H}}|x\rangle}{\int \lim_{\beta\to\infty} \langle x|e^{-T\hat{H}}|x\rangle\, dx}\right)^{\frac{1}{2}} \qquad \ldots(42)$$

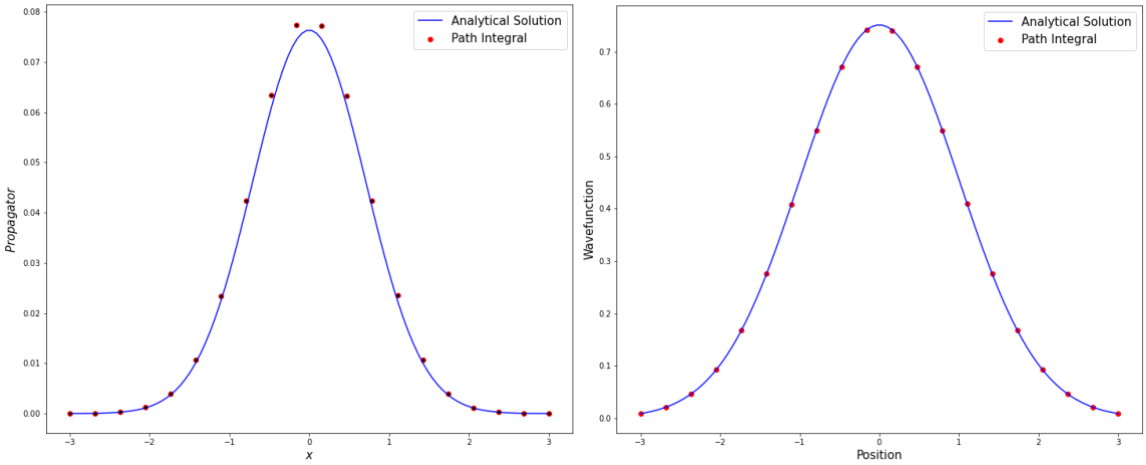

Figure 1 (left): The propagator for a quantum harmonic oscillator in the ground state. It was obtained by evaluating the path integral numerically using the 'vegas' package in python for 10^5 *iterations,* 8 *time steps of lattice size* 0.5*, and the mass, m, frequency ω and ħ set to* 1.

Figure 2 (right): The wavefunction for a quantum harmonic oscillator in the ground state calculated using the propagator in figure 1. We obtain the expected gaussian distribution as numerical values exhibit excellent agreement with the analytical solution.

Figures 1 and 2 demonstrate the use of propagators to compute physical properties of the quantum system. As detailed before, in general, propagator-like objects known as correlation functions allow computation of any physical property of a quantum system.

5.2. MCMC

1. Quantum harmonic oscillator

We now perform the MCMC computations for the potential $V(x_j) = \frac{m\omega^2 x_j^2}{2}$ for the ground state and the first excited state. We also find the ground state wavefunction using (42).

a. Ground state wavefunction

While figure 2 was plotted using a standardized library to directly compute the path integral, figure 3 illustrates the same analysis done using the MCMC method. We observe a clear equivalence in the results, and thus, have convincing evidence to proceed with our analysis of the unperturbed and perturbed energies.

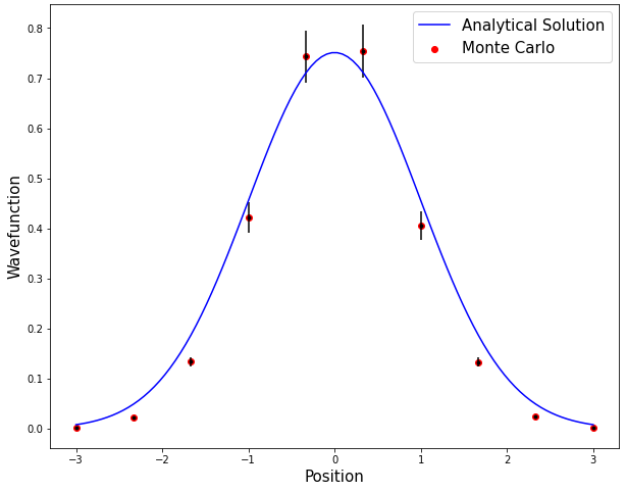

Figure 3: The wavefunction for a quantum harmonic oscillator in the ground state calculated using MCMC method for 5000 *paths with* 20 *lattice points; spacing =* 0.9*. The plot illustrates an equivalence with figure 2, thereby demonstrating the equivalence between MCMC method and direct solution to the Path Integral.*

Our MCMC method lacks optimization to increase computational speeds. In light of our computational equipment, an average over only 5000 paths was feasible. Thus, we observe significantly larger error bars, as well as deviation from the analytical result in figure 3 compared to figure 2 where 10^5 paths were used.

b. Ground state energy

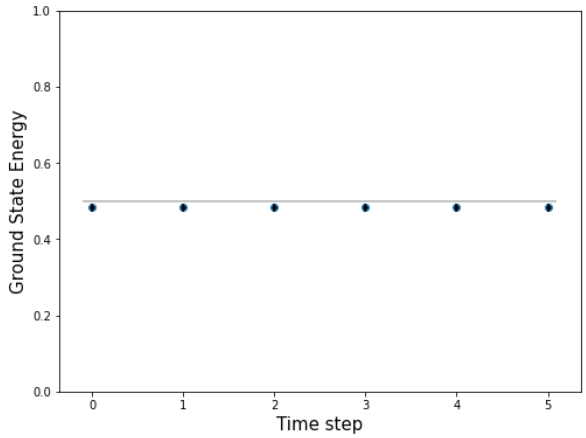

Figure 4: Convergence of the ground state energy with time steps for the quantum harmonic oscillator computed using the MCMC method. We get approximately $E_0 = 0.49 \pm 0.01$ *in units of ħ. The horizontal line indicates the analytical ground state energy* $\tilde{E}_0 = 0.50$*. MC average over* 10^4 *paths;* 20 *lattice points;* 0.5 *lattice spacing;* $\epsilon = 1.4$ *;* $N_{\text{cor}} = 20$*. The error bars indicate underestimation of statistical errors.*

We obtain the ground state energy of the quantum harmonic oscillator as $E_0 \approx 0.49 \pm 0.01$. The ground state energy does not vary with time steps as expression (33) shows that the entire path is used for computing a single number as the correlation function. Therefore, we do not observe any explicit convergence.

c. First excited state energy

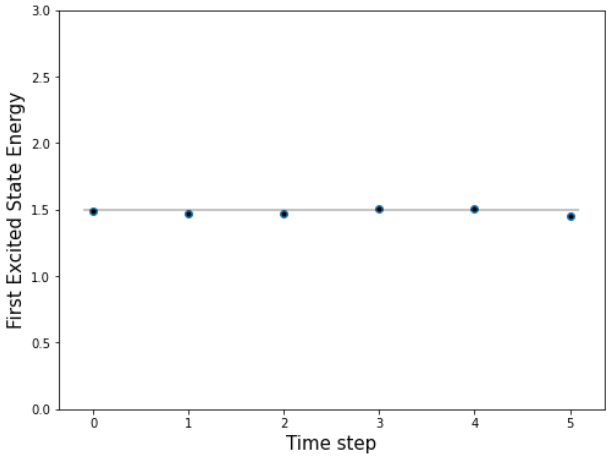

Figure 5: Convergence of the first excited state energy with time steps for the quantum harmonic oscillator computed using the MCMC method. We get approximately $E_1 = 1.50 \pm 0.01$ *in units of ħ. The horizontal line indicates the analytical energy* $\tilde{E}_1 = 1.50$. *MC average over* 10^4 *paths;* 20 *lattice points;* 0.5 *lattice spacing;* $\epsilon = 1.4$; $N_{\text{cor}} = 20$.

We obtain the first excited state energy of the quantum harmonic oscillator as $E_1 = 1.50 \pm 0.01$. The MC result converges quickly at the first time step. However, the results diverge for larger time steps. Thus, accounting for this convergence and divergence behavior, we select only the time step = 0 values for all results in the anharmonic potential case.

2. Quartic-anharmonic oscillator

We now perform the MCMC computations for the potential $V(x_j) = \frac{m\omega^2 x_j^2}{2} + \lambda x_j^4$ for the ground state and the first excited state with varying values of λ and compare the results with the corresponding perturbative solutions derived in section 2.3. We make the comparison for both, the first and second order perturbation theory. Finally we illustrate the asymptotic nature of the ground state perturbative expansion and discuss the limit within which it is valid.

a. Ground state energy

MC average over 5000 paths; 20 lattice points; 0.4 lattice spacing; $\epsilon = 1.4$; $\mathrm{N}_{\text{cor}} = 20$.

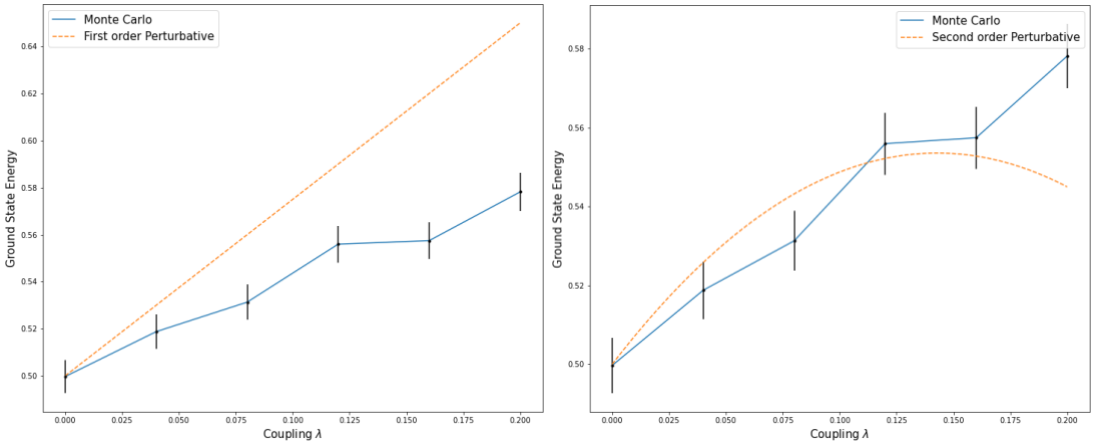

Figure 6: Comparison of the MCMC solutions and the first and second order perturbative solutions for the ground state energy of the quartic anharmonic oscillator with varying perturbative coupling λ. The perturbative solutions diverge for approximately $\lambda > 0.075$ while the MCMC solutions remain stable. Within the error bars, the MCMC solutions indicate a smooth increase in the ground state energy for increasing coupling λ.

For very small λ, the perturbative and MCMC solutions have close agreement. As expected, within this range, the second order perturbative solution has better agreement with the MCMC solutions as compared to the first order. The second order solution also indicates that the perturbative solutions are stable only for approximately $\lambda < 0.075$. However, the MCMC solutions indicate a steady increase with increasing coupling. We verify this for a larger range of coupling in figure 7.

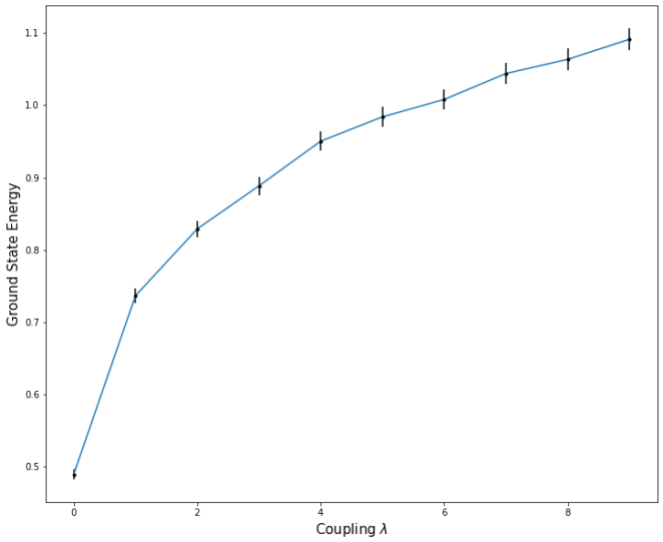

Figure 7: MCMC solutions for the ground state energy of the quartic anharmonic oscillator with varying perturbative coupling λ. The energy solutions have a non-linear stable increase with increasing coupling even for large values of λ.

For $\lambda \to 0$, the perturbative and the MCMC solutions converge to the harmonic oscillator ground state energy, $E_0 = 0.5$.

b. First excited state energy

MC average over 5000 paths; 20 lattice points; 0.5 lattice spacing; $\epsilon = 1.4$; $N_{cor} = 20$.
Note that we're finding the difference between E_1 and E_0, that is ΔE_1, and not the absolute value for E_1.

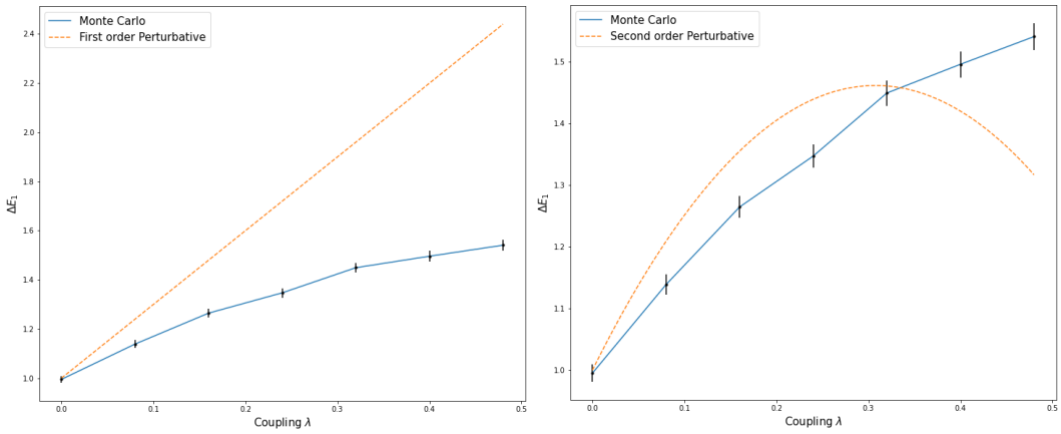

Figure 8: Comparison of the MCMC solutions and the first and second order perturbative solutions for the difference between the first excited and ground state energy of the quartic anharmonic oscillator with varying perturbative coupling λ. The perturbative solutions diverge for approximately $\lambda > 0.2$ while the MCMC solutions remain stable.

Again, for small λ, the perturbative and MCMC solutions have close agreement with the second order perturbative solution having better agreement with the MCMC solutions as compared to the first order. The second order solution also indicates that the perturbative solutions are stable only for approximately $\lambda < 0.2$. However, the MCMC solutions indicate a steady increase with increasing coupling. We verify this for a larger range of coupling in figure 9.

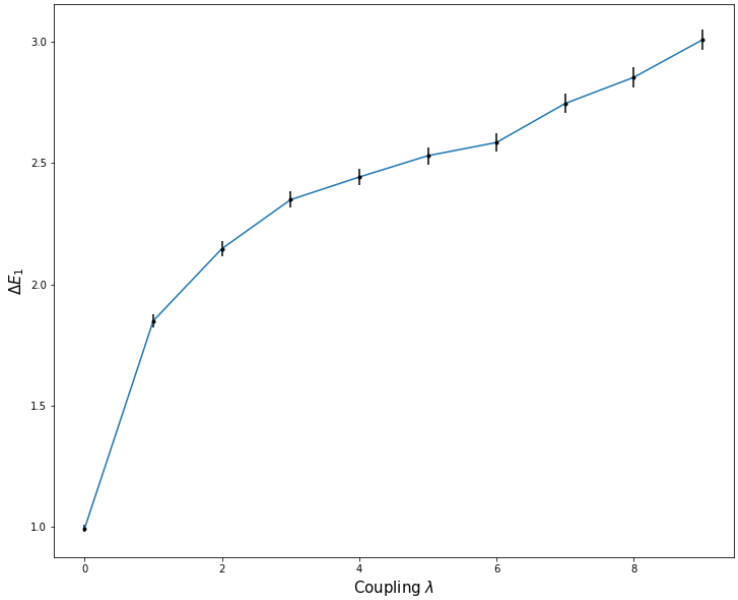

Figure 9: MCMC solutions for ΔE_1 of the quartic anharmonic oscillator with varying perturbative coupling λ. The energy solutions have a non-linear stable increase with increasing coupling even for large values of λ.

For $\lambda \to 0$, the perturbative and the MCMC solutions converge to the harmonic oscillator case, $\Delta E_1 = 1.0$.

c. Asymptotic expansion of ground state energy

The perturbative solutions for the ground state in figure 6 indicate a range of λ for which these solutions may be valid approximations. Naively, from the perturbation theory, it seems we should be able to make better approximations and increase the range of λ for which the solutions might be valid by solving higher and higher order perturbative solutions. However, as explained in section 2.3 using expression (22), the perturbative expansion for the ground state is an asymptotic expansion. We illustrate this in figure 10.

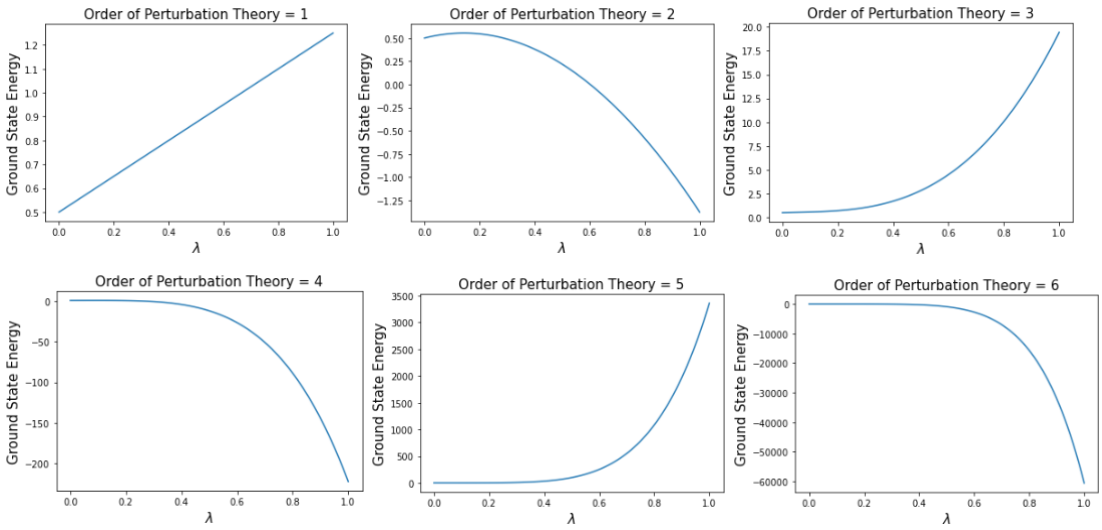

Figure 10: n^{th} order perturbative solution for the ground state energy of the quartic anharmonic oscillator. The expansion is asymptotic and does not converge even for lower order solutions.

Clearly, the asymptotic effects are very large for $\lambda \approx 1$. Thus, we undertook two remedies for this. First, we considered the perturbative solution only for $\lambda < 0.2$. Next, we calculated successive terms in the expansion and truncated the series when successive terms began increasing. By these standards, we determined the second order solution as the most appropriate solution for our case. Thus, in our analysis for the ground state, we used only the second order perturbative solution despite having the higher order corrections.

6. Discussion

Our results for the MCMC simulations have strong agreement with the analytical values of the quantum theory, and provide a robust, albeit computationally expensive, mechanism for computing solutions when analytical solutions are not possible. It has also verified an equivalence between the analytical path integral and the Monte Carlo computations, which are fundamentally statistical analogues of the quantum theory. Thus, we have successfully explored an alternate approach for calculating properties of the quantum theory by formulating the problem in the path integral framework, making the analogy with the canonical ensemble, and then computing Monte Carlo integrals. Of course, in practice, such an exercise would be an overkill to solve a system like the quantum harmonic oscillator where analytical solutions exist. However, for anharmonic oscillators, our results have demonstrated greater reliability of this method compared to perturbative analysis.

This approach becomes more important in fields where the path integral framework is more widely used, such as lattice QCD. Our future aim is to apply this approach to a classical open string which models the interactions between a quark-antiquark pair. The challenge would involve discretizing the string Lagrangian while preserving its reparameterization invariance.

In order to use this approach for different systems, we will have to rigorously develop a method to determine the simulation parameters– the number of lattice points; the lattice spacing; the quantum fluctuation parameter, ϵ; the correlation parameter, N_{cor}; the thermalization time; etc. Since we had a well-studied system for the current work, we were able to refer to existing literature for optimum parameters. This may not be possible for novel applications.

7. References

[1] Lepage, Peter G. (2005), Lattice QCD for Novices

[2] Shikhar Mittal et al 2020, Path integral Monte Carlo method for the quantum anharmonic oscillator, *Eur. J. Phys. 41 055401* https://iopscience.iop.org/article/10.1088/1361-6404/ab9a66

[3] B. Zweibach (2018), Lecture notes, *Chapter 1. Perturbation Theory, Quantum Physics III Spring 2018, MIT* https://ocw.mit.edu/courses/physics/8-06-quantum-physics-iii-spring-2018/lecture-notes/MIT8_06S18ch1.pdf

[4] Dhania, Sourav (2019), Monte Carlo Simulation of Harmonic Oscillator using Metropolis Algorithm in Discrete Euclidean Time, *IISER Mohali https://web.iisermohali.ac.in/Faculty/anoshjoseph/internships/2019/report_2019_Saurav_Dhania.pdf*

[5] Rodgers, Ronnie (2014), Monte Carlo Simulation of Harmonic Oscillator using Metropolis Algorithm in Discrete Euclidean Time, *DESY Summer Student Program, https://www-zeuthen.desy.de/students/2014/reports/RodgersRaes.pdf*

[6] Griffiths, D. J. (2005). Introduction to quantum mechanics. *2nd, Pearson, Chapter2. The time-independent Schrodinger equation,* 90-91.

[7] Feynman, R. P. (1965). Feynman lectures on physics. Volume 3: Quantum mechanics.

[8] Bender, C. M., & Wu, T. T. (1969). Anharmonic oscillator. *Physical Review, 184(5), 1231.*